Proceedings of International Symposium on

NONLINEAR TRANSPORT AND RELATED PHENOMENA IN INORGANIC QUASI ONE DIMENSIONAL CONDUCTORS

Hokkaido University

Sapporo, Japan

20-22 October, 1983

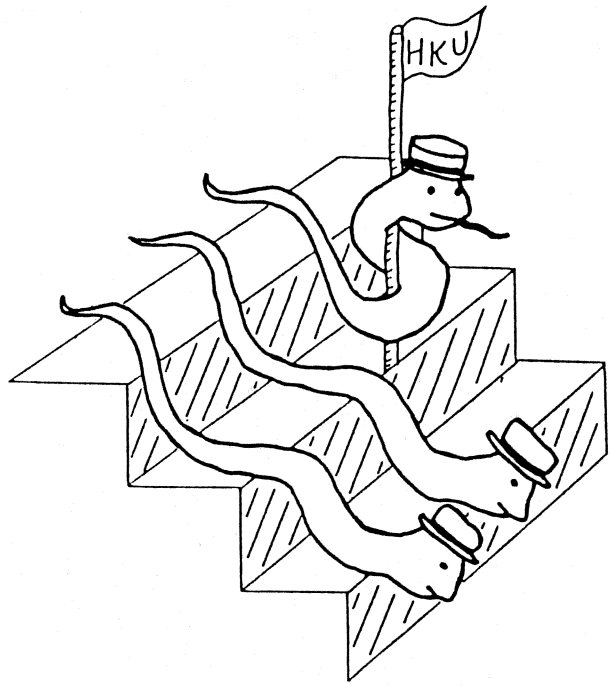

OSCILLATIONS, INTERFERENCE EFFECTS, AND SWITCHING IN CHARGE DENSITY WAVE SYSTEMS

A. Zettl
Department of Physics, University of California, Berkeley
Berkeley, California 94720

Abstract

Many low dimensional metals are subject to periodic lattice distortions at low temperatures. In several instances, the resulting charge density wave (CDW) is mobile and contributes to the electrical dc and ac conductivity. Often the onset of dc conduction is associated with a sharp hysteretic switch from the non-conducting (pinned) to the conducting (sliding) CDW state. Associated with the conducting state are coherent and incoherent current oscillations. The coherent oscillations may interact with externally applied ac signals, leading to strong interference effects. In this presentation the properties of the oscillations, interference effects, and switching are discussed for the CDW systems $NbSe_3$ and orthorhombic TaS_3. Analysis of the experiments is based on models of classical motion or quantum tunneling of the CDW condensate.

1. INTRODUCTION

The $2k_F$, T = 0 divergence of the generalized susceptibility of a one dimensional electronic system can lead to a number of interesting ground states. One possibility is the charge density wave (CDW) state, associated with a periodic lattice distortion of wavevector $Q = 2k_F$ and a consequent spatial modulation of the electronic charge density. A CDW corresponds to an electron-hole pairing in k space, and the charge density may be described by $\langle c^{\dagger}_{k+Q} c_k \rangle$, where $c^{\dagger}$ and c refer respectively to electron creation and annihilation operators. With V the interaction potential, the CDW order parameter becomes

$$\Delta_k = \sum_{k'} V_{kk'} \langle c^{\dagger}_{k'+Q} c_k \rangle \qquad (1)$$

For a strictly one-dimensional system, a CDW transition is possible only at T = 0. However, for a quasi one-dimensional material, interchain coupling allows for a CDW state at finite temperatures. This state corresponds to a three-dimensional ordering of the system.

In real materials, CDW distortions at low temperatures are a common occurence, and in fact a CDW ground state turns out to be the rule, rather than the exception, for a wide class of inorganic and organic conductors. The static properties of CDW formation, e.g. the periodic lattice distortion resulting in a gap in the single-particle excitation spectrum, are fairly well understood. Consequent changes in the conventional transport coefficients, such as changes in the electrical resistivity, Hall constant, or thermoelectric power, can also be well accounted for. The most intriguing, and most poorly understood, aspect of CDW systems appears to be the dynamical properties of the CDW condensate itself. Early (1976) measurements[1] on the CDW conductor NbSe- showed highly non-linear dc conductivity, and subsequent transport studies[2-5] have revealed strongly frequency-dependent ac conductivity, and coherent and incoherent current oscillations in

the non-linear conductivity region.[6,7] These properties represent a collective motion of the CDW condensate. Similar properties are observed in the related trichalcogenides monoclinic TaS_3 and NbS_3, and also in the linear chain compounds $(TaSe_4)_2I$, $(NbSe_4)_{3.33}I$, and $K_{0.3}MoO_3$.[8] The theoretical investigation of CDW transport phenomena dates back nearly 30 years, to a study of superconductivity by Frohlich.[9] Frohlich's approach, although not applicable to superconductivity, has formed the basis for a number of recent models of collective CDW motion. Among these models are descriptions in which the CDW is treated as a classical object (with[10] or without[11] internal degrees of freedom) in a periodic potential, or quantum formulations where the CDW contributes to the electrical conductivity by macroscopic quantum tunneling.[12] The possibility of macroscopic quantum phenomena at temperatures near 300 K makes the CDW dynamics problem all the more interesting.

Here we shall investigate several unusual transport properties of the CDW state, namely coherent oscillations, interference effects between coherent current oscillations and applied rf electric fields, and switching phenomena associated with the onset of CDW conduction. We shall limit our discussion to the CDW materials $NbSe_3$ and orthorhombic TaS_3, although we note that $(TaSe_4)_2I$, $(NbSe_4)_{3.33}I$, and $K_{0.3}MoO_3$ display similar properties.

2. OSCILLATION PHENOMENA

Fleming and Grimes[6] were the first to observe that non-linear CDW conduction occurs only after a well-defined threshold electric field E_T is exceeded. In the non-linear conductivity region, an unusual amount of broad-band noise, along with periodic current oscillations rich in harmonic content, is observed. This is shown in Fig. 1. The sharp peaks in the Fourier spectrum have been termed "narrow-band noise". It has been suggested that the oscillations and associated narrow band noise arise from the sliding of the CDW over the peaks and valleys of the potential

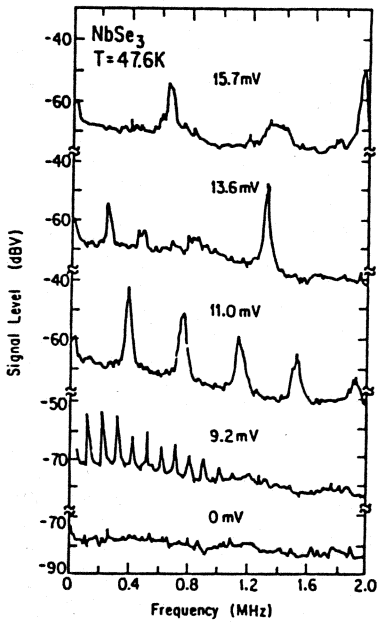

FIG. 1
Resonse spectrum of $NbSe_3$ for various values of the dc bias voltage. The narrow-band noise peaks move to higher frequencies with increasing bias. (ref. 6)

that pins the phase of the wave. In this case the current oscillations reflect the time dependent velocity of the CDW condensate. The observation of narrow-band current oscillations (or voltage oscillations, when the sample is driven by a current source) is then in itself rather remarkable, for it indicates a highly coherent response of the whole crystal. If different CDW regions responded individually, the phase average of the oscillating currents would give a time independent response.

2.1 Harmonic Content of the Oscillations

Studies[13,14] have shown that the noise spectrum contains at least eight harmonics, and that the noise peaks are extremely sharp, with quality factors of the order 10^3-10^4. A typical noise spectrum for a high quality $NbSe_3$ sample is shown in Fig. 2a. The finite width of the peaks in this figure is instrumental. Fig. 2b shows a similar spectrum for orthorhombic TaS_3 in the non-linear CDW state. From Figs. 2a and 2b it is evident that the first peak at frequency f_1 is the dominant one, with higher harmonics falling off in amplitude with the order of the harmonic.

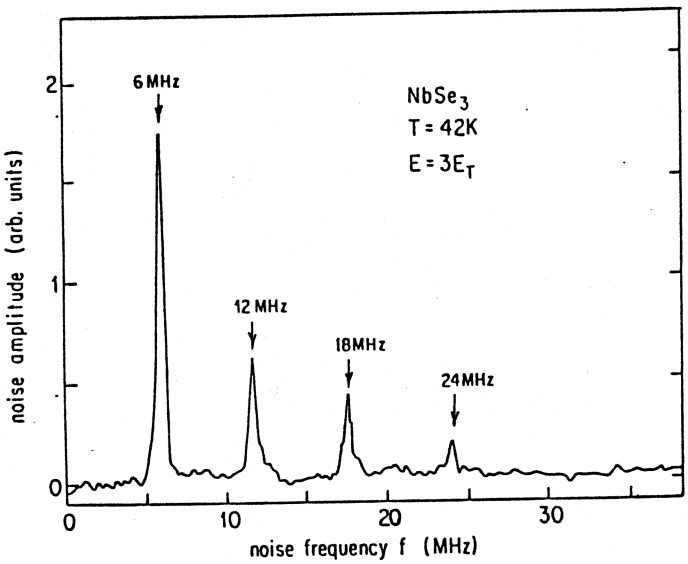

Fig. 2a
Narrow-band noise spectrum of $NbSe_3$ in the non-linear conductivity region. The vertical amplitude scale is in linear units.

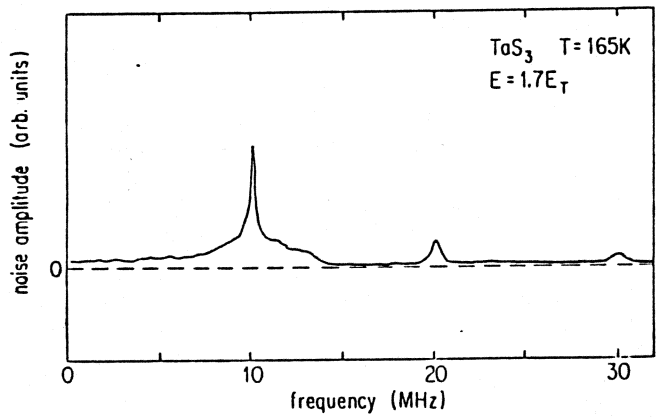

Fig. 2b
Narrow-band noise spectrum of TaS_3 in the non-linear conductivity region. The vertical amplitude scale is in linear units.

In a simple phenomenological model of CDW transport developed by Gruner, Zawadowski, and Chaikin[11], the CDW condensate is represented by a charged classical object in a periodic potential. The equation of motion, assuming a sinusoidal potential, is

$$\frac{d^2x}{dt^2} + \frac{1}{\tau}\frac{dx}{dt} + \frac{\omega_0^2}{Q}\sin Qx = \frac{eE}{m^*} \qquad (2)$$

where x is the CDW position, $1/\tau = \gamma/m^*$ with γ the damping constant and m^* the effective mass of electrons in the CDW state, and $Q = 2\pi/\lambda$ where λ is the CDW wavelength. E is the driving field. This equation describes the overall features of the field and frequency dependent conductivity of $NbSe_3$ and TaS_3, as discussed elsewhere in this volume.[15] Eq.(2) also predicts narrow-band noise in the non-linear conductivity region, with Fourier components of the excess current at

$$I_n \sim [\alpha^2-1]^{1/2}\,[\alpha - (\alpha^2-1)^{1/2}]^n \cos\left[n\left(\omega t + \frac{\pi}{2} + \sin^{-1}\alpha \right)\right] \qquad (3)$$

where $\alpha = E/E_T$ and n = 1, 2, 3, ... Eq.(3) is valid only in the overdamped limit, where the acceleration term in Eq.(2) is neglected. Eq.(3) predicts a decrease in noise amplitude for higher harmonics, as observed experimentally. However, as first pointed out by Monceau et al[16], the fall-off is to fast for large α. This is illustrated in Fig. 3 where Eq.(3) has been fitted to the narrow-band noise spectra of TaS_3 and $NbSe_3$. Near $\alpha = 1.7$ the fit is very good, while for $\alpha = 3$ the agreement with experiment is less convincing. Better fits can be obtained, however, with slight modifications of the pinning potential term in Eq.(2).

2.2 Current-Frequency Relation

Experimentally, the fundamental oscillation frequency f_1 increases with increasing E, and consequently f_1 increases with increasing I_{CDW}, where I_{CDW} is the time averaged excess current carried by the condensate. In a very general sense we may write the excess current as

$$I_{CDW} = n_c e\, v_d A \qquad (4)$$

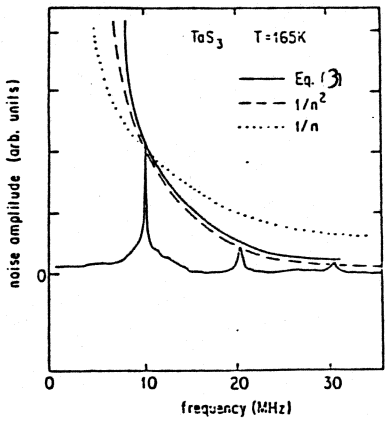

Fig. 3a
Harmonic amplitude decay of narrow-band noise peaks in TaS_3. The solid line is Eq.(3) normalized to the first noise peak. Also shown are first and second power roll-offs.

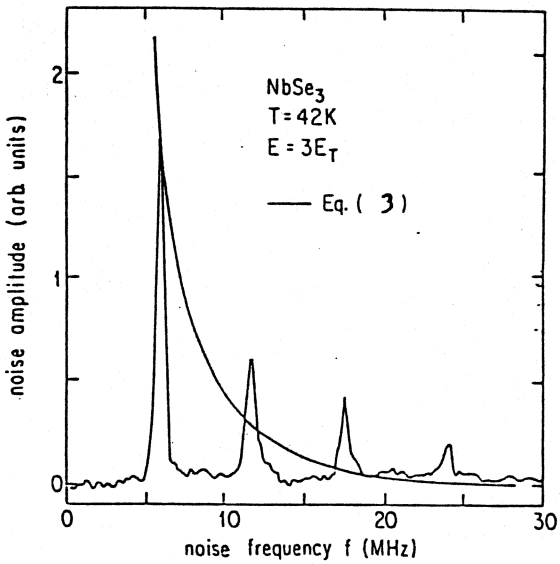

Fig. 3b
Harmonic amplitude decay of narrow-band noise spectrum in $NbSe_3$. The solid line is Eq.(3), normalized to the first frequency peak.

where n_c is the density of electrons condensed in the CDW state, v_d is the CDW drift velocity, and A is the cross-sectional area of the sample. With $v_d = f_1\lambda$, Eq.(4) becomes

$$I_{CDW} = n_c e A\lambda f_1 \qquad (5)$$

Hence, f_1 is directly proportional to I_{CDW}, as first proposed by Monceau et al.[17] This proportionality has been verified in $NbSe_3$[18] and TaS_3[14] well into the MHz frequency region, as illustrated in Fig. 4.

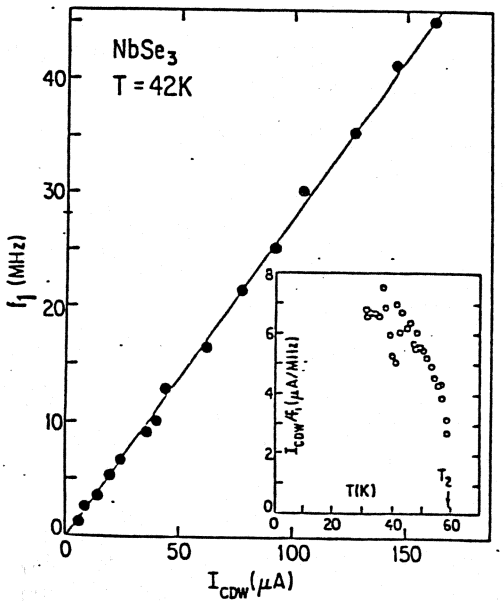

Fig. 4a
Frequency of fundmental noise peak versus excess CDW current in $NbSe_3$. The linear relation supports Eq.(5). The inset shows the I_{CDW}/f_1 slope for various temperatures below T_p.

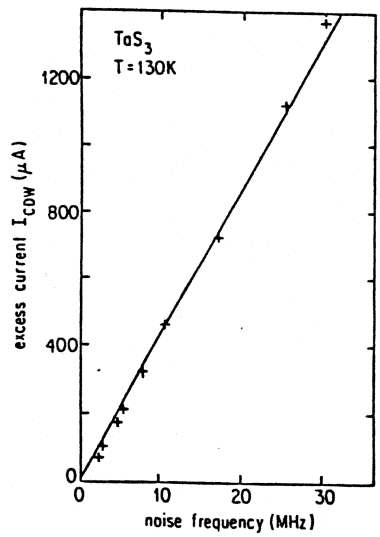

Fig. 4b
Fundamental noise frequency versus excess CDW current in TaS_3. The linear relation supports Eq.(5).

The slope of the I_{CDW} vs. f_1 line is useful in determining λ if n_c is known, and conversely n_c if λ is known. For $NbSe_3$ n_c has been determined from Hall effect studies[19], $n_c = 10^{21}$ cm^{-3}. However, the ungapped portion of the Fermi surface in $NbSe_3$ makes the assumed value of $n_c(T = 0)$ unreliable. This, in turn, makes λ difficult to evaluate from Eq.(5) for $NbSe_3$. In TaS_3, however, Fermi surface destruction at T_P is complete. From the known lattice parameters[20] and the original band filling (1/4), we find $n_c(T = 0) = 2.6 \times 10^{21}$ cm^{-3}. This value is easily corrected for finite temperature effects using the temperature dependence of the CDW order parameter, as determined from X-ray studies.[21] We thus obtain $n_c(T = 130\ K) = 1.9 \times 10^{21}$ cm^{-3}. Combining this number with the slope given in Fig. 4b, Eq.(5) yields $\lambda = 13.26$ A, in excellent agreement with the CDW wavelength determined from the X-ray analysis, $\lambda = 13.3$ A. Hence the period of the pinning potential in TaS_3 corresponds to the CDW wavelength. In this case Eq. (2) may be restated as

$$\frac{I_{CDW}}{f_1} \text{ per chain} = 2e \qquad (6)$$

2.3 Amplitude of the Oscillations

The amplitude of the current oscillations depends on both the applied field E and on the sample volume.[22] Here we consider only the E dependence. Fig. 5 shows the amplitude of the fundamental f_1 noise peak in TaS_3, as a function of dc bias. The amplitude clearly increases with increasing E up to approximately $E = 2E_T$, whereafter it slowly decreases. Eq.(2) predicts an amplitude A_1 for the first frequency peak

$$A_1(E) \sim \left[\left(\frac{E}{E_T}\right)^2 - 1\right]^{1/2} \left[\frac{E}{E_T} - \left\{\left(\frac{E}{E_T}\right)^2 - 1\right\}^{1/2}\right]. \qquad (7)$$

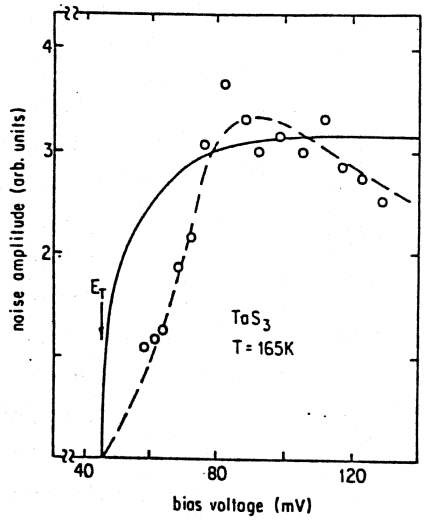

Fig. 5
Amplitude of fundamental noise peak versus bias voltage in TaS_3. The solid line is Eq.(7).

The full line in Fig. 5 is Eq.(7), normalized to $A_1(V = 80\ mV) = 3$. It is apparent that the amplitude of the fundamental increases much more slowly with increasing electric field than that predicted by Eq.(2). The rapid increase predicted by the model is related to the rapid increase of I_{CDW} predicted just above threshold, and to the consequent divergence of the differential conductivity dI_{CDW}/dE predicted as E approaches E_T from above.[23] This divergence is not observed by experiment, and I_{CDW} is found to increase slowly with increasing E above E_T, with a functional form suggestive of a tunneling phenomenon. An amplitude of the fundamental noise peak proportional to the observed I_{CDW} would lead to the measured increase of A_1 as seen in Fig. 5.

In the high-field limit the amplitude of the fundamental decreases with increasing E, again in contrast to the prediction of Eq. (7). This may be related to an inertial effect. A classical harmonic oscillator model with inertia can, under various conditions, lead in the high field limit to a decreasing oscillation amplitude with increasing E. This has been discussed by Ben-Jacob.[24] A theory of the coherent current oscillations in $NbSe_3$ by Bardeen[18] also emphasizes the role of an inertial term. The theory does not depend on the details of the model, but requires only that the CDW slide without additional dissipation over the hills and valleys of the pinning potential. Pinning is described by a pinning potential $V(\phi)$, where ϕ is the phase of the wave relative to that of the potential at V(0). The theory

suggests that current oscillations result from the CDW moving adiabatically over the varying potential in such a way that the total energy of the wave, kinetic plus potential, is constant. If the velocity of the wave is $v_d + v_1(\phi)$, where v_d is the average velocity and v_1 is the periodic part that gives the oscillating current, then energy conservation requires

$$\frac{1}{2} m^*(v_d+v_1)^2 + V(\Phi) = \text{const.} = \frac{1}{2} m^* v_d^2 . \tag{8}$$

Thus, if $v_d >> v_1$,

$$V(\Phi) = -m^* v_d v_1(\Phi) \tag{9}$$

which implies that the current oscillations, given by v_1, should be inversely proportional to the drift velocity v_d. As $I_{CDW} = n_c e v_d A$, the oscillating current $\Delta I = n_c e v_1 A$. Eq.(9) then leads to

$$\Delta I \times I_{CDW} = -V(\Phi)/m^* n_c^2 e^2 A^{-2}. \tag{10}$$

Hence, in the high field limit, the oscillation amplitude ΔI should decrease, and $\Delta I \times I_{CDW}$ should tend to a constant. This is observed experimentally[18], as illustrated in Fig. 6 for $NbSe_3$.

2.4 Time Dependence of the Oscillations

Fleming[25] was the first to demonstrate that coherent voltage oscillations associated with a rectangular current pulse exceeding threshold could be synchronized to the start of the pulse. If the voltage is displayed on an oscilloscope, the oscillations appear stationary, and may thus be directly viewed in the time domain. Fig. 7 shows the oscillations in $NbSe_3$ for two values of the

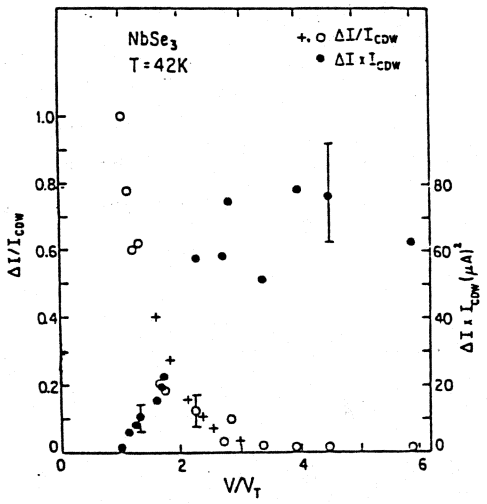

Fig. 6
Fraction of oscillating current to total excess CDW current in $NbSe_3$. Near threshold the oscillating portion constitutes 100% of the total excess current. Also shown is the product of oscillating current and total excess current. In the high-field limit, this product tends to a constant (see Eq.(10).

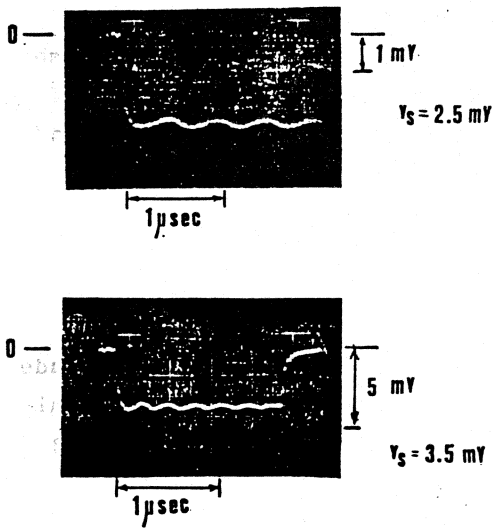

Fig. 7
Real time display of voltage oscillations in $NbSe_3$ induced by a constant current pulse. The oscillation amplitude decreases in time following the start of the pulse. The voltage displayed represents the total voltage across the specimen. V_s is the time averaged voltage during the pulse.

driving current. The fundamental frequency f_1 and the amplitude of the oscillations are clearly resolved. The oscillations are remarkably "clean" and do not fluctuate in phase. The static appearance of the traces on the oscilloscope indicates a high

degree of reproducibility for the traces (the oscilloscope was triggered by the pulse generator and not by the oscillations themselves). A single pulse is found to generate the same trace, and thus the oscilloscope display is not a time average of waveforms with randomly varying phases.

From Fig. 7, the amplitude of the waveforms is clearly time dependent, with the amplitude decreasing in time following the start of the current pulse. It however does not decrease to zero at time $t = \infty$; rather a limiting value for the amplitude is approached. This limiting value is what is normally observed using the standard spectrum analyzer method of detection. We may suggest an empirical equation for the oscillation amplitude of the form

$$\Delta V(t) = \Delta V(t=0)\left[a+b\ e^{-tf_1\Gamma}\right] \qquad (11)$$

where a, b, and Γ are dimensionless constants. Analysis of many different traces for $NbSe_3$ at T = 42 K indicates a = 1/4, b = 3/4, and Γ = 1/4.5. The time dependence of the oscillation amplitude may represent a time dephasing of various CDW domains within the specimen, where phases are locked only at t = 0 due to the initial current pulse propagation.

2.5 Temperature Dependence of the Oscillations

In both $NbSe_3$ and TaS_3 the oscillation characteristics are strongly temperature dependent. Of interest is $n_c(T)$, the concentration of carriers condensed in the CDW state. From Eq.(5), $n_c = I_{CDW}/eA\lambda f_1$. Hence the ratio I_{CDW}/f_1 is a direct measure of n_c, and consequently also the energy gap $\Delta(T)$. n_c and Δ are related by[26]

$$n_c(T) = n_c(T=0)\ 7\zeta(3)[|\Delta(T)|/2\pi T_p]^2 \qquad (12)$$

where $\zeta(3)$ is the third order zeta function. Fig. 8 shows the ratio I_{CDW}/f_1 as a function of temperature for $NbSe_3$. Also plotted are the CDW order parameter as determined from X-ray scattering data[27] and the BCS expression for $\Delta(T)$. The ratio I_{CDW}/f_1 indeed falls toward zero as T approaches T_P from below, as predicted by Eq.(12). At temperatures below approximately 45 K, the scatter in the I_{CDW}/f_1 data becomes abnormally large. This may be related to metastable states in $NbSe_3$, discussed elsewhere in this volume.[28] A plot of I_{CDW}/f_1 for TaS_3 is presented in Fig. 9.

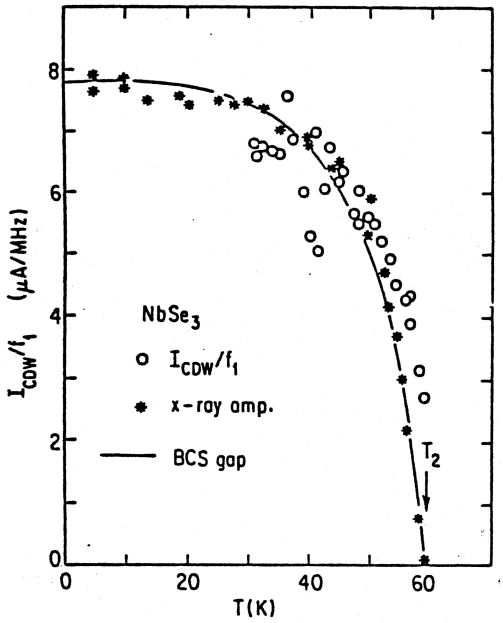

Fig. 8
Temperature dependence of I_{CDW}/f_1 ratio in $NbSe_3$. This ratio reflects n_c. Also shown are the X-ray superlattice amplitudes (ref. 27) and the BCS expression for the energy gap.

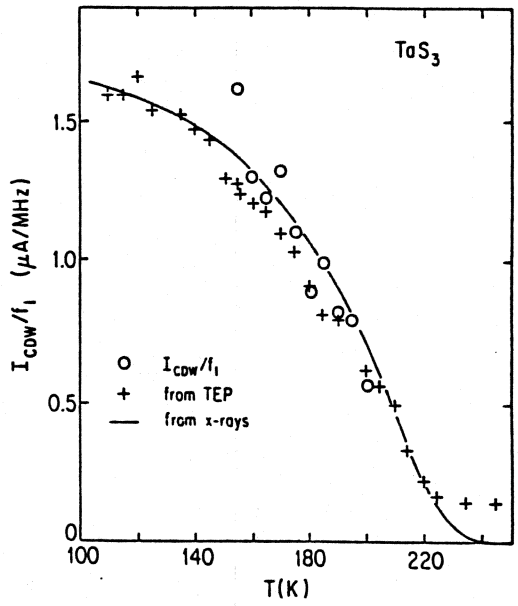

Fig. 9
Temperature dependence of I_{CDW}/f_1 ratio in TaS_3. The energy gap, as determined from thermoelectric power and X-ray measurements (ref. 21), is also shown.

2.6 Other Models for the Oscillations

A number of models have been proposed to account for the coherent current or voltage oscillations discussed above. One such model is that of a relaxation oscillator.[13,29] It predicts an oscillating component for the CDW current, with higher harmonics in the power spectrum. In this electrical analog model of CDW response the CDW's are represented by relaxation oscillators which lock together in phase due to a weak resistive or capacitive coupling. A simplified example of such an electronic circuit is shown in Fig. 10. The resulting current waveform is periodic in time and rich in harmonics. For a suitable choice of circuit components, the current waveform of the oscillations resembles well the current oscillations observed in $NbSe_3$, with a closely corresponding narrow-band noise spectrum in the frequency domain. The model also accounts for the linear relation between I_{CDW} and f_1.

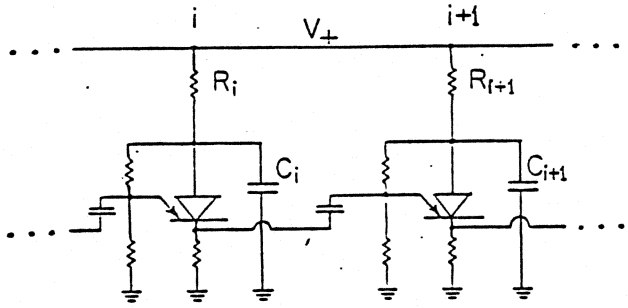

Fig. 10
Electronic analog of CDW system. The analog consists of a linear array of coupled relaxation oscillators. (ref. 13)

Recently, Bak[30] has suggested that the current oscillations in $NbSe_3$ are due to motion of a soliton lattice, where peaks in the current oscillation represent motion of individual solitons past the current detector at the end of the sample. In the model the CDW is commensurate over most of the volume ($\lambda = 4a$, with a the lattice constant), with the extra charges corresponding to the difference from commensurability going into solitons or discommensurations that form a regular lattice with spacing L. The current per chain may be written as $I = e^*v/L = e^*f_1$, where f_1 is the oscillation frequency, v is the soliton velocity, and e^* is the charge in length L. For the soliton lattice appropriate to $NbSe_3$ $e^* = e/2$, and thus the solitons carry fractional charge. Hence the ration I/f_1 may be written as

$$\frac{I_{excess}}{f_1} \text{ per chain} = \frac{e}{2} \qquad (13)$$

The strong temperature dependence of I/f_1 as shown in Fig. 8 suggests that in the soliton model the fractional charge of the solitons is temperature dependent. This is inconsistent with the formulation of the soliton model and thus transport by sliding CDW's is favored. It is possible, however, that a soliton lattice could exist if the entire CDW system, including solitons, moved under the influence of an electric field.

Barnes and Zawadowski[31] have presented a theory in which the CDW is considered as a superposition of two macroscopic quantum states characterized by $\pm Q$. The two coherent states are composed of electron-hole pairs with total momentum $\pm Q$, and the motion of the CDW at constant velocity v leads to a splitting of the Fermi levels corresponding to the two macroscopic quantum states. An oscillating current results at frequency $f = 2Qv$. This suggests $e^* = e$, hence

$$\frac{I_{CDW}}{f_1} \text{ per chain} = e \qquad (14)$$

The Barnes-Zawadowski approach predicts that the dominant peak in the noise spectrum is at $2f_1$, rather than at f_1. This is not observed in Fig. 2, where the f_1 peak is clearly dominant for both $NbSe_3$ and TaS_3.

Other models for oscillations in CDW systems include a phase vortex description by Ong and Maki.[32] This model is described elsewhere in this volume.[33]

3. INTERFERENCE EFFECTS

We shall here consider the response in $NbSe_3$ and TaS_3 when an excitation of the form

$$V = V_{dc} + V_{ac}\cos(\omega t) \tag{15}$$

is applied to the sample. Of particular interest will be interference effects when the frequency of coherent current oscillations equals $\omega/2\pi$.

3.1 Dc I-V Characteristics in the Presence of rf Radiation

The non-linear I-V characteristics of both $NbSe_3$ and TaS_3 are influenced by the application of an rf field. The observed response is a sensitive function of the amplitude V_{ac} and frequency ω of the rf field. Monceau et al[17] were the first to demonstrate interference effects in $NbSe_3$, by measuring the differential dc resistance in the presence of an applied rf electric field. With high quality crystals, the effects can be observed directly in the I-V characteristics, as shown in Fig. 11. For $V_{ac} = 0$, a smooth, non-linear I-V curve is observed. At higher values of V_{ac}, well-defined steps appear in the non-linear conductivity region. We shall define the original step in the I-V

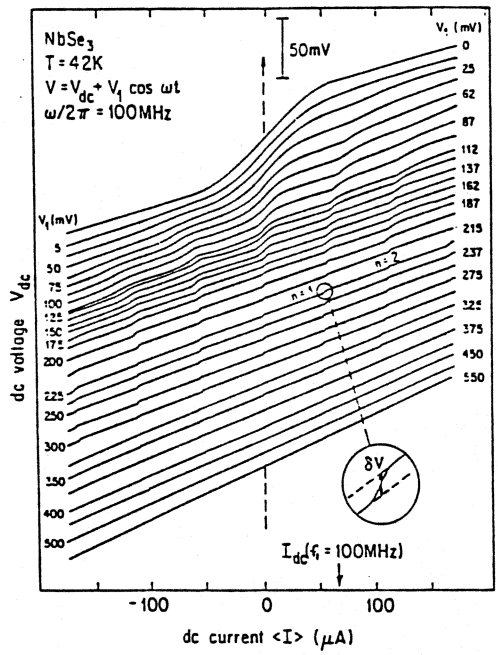

Fig. 11
d-c I-V characteristics of $NbSe_3$ in the presence of rf radiation. Shapiro steps are induced whenever the frequency of the intrinsic current oscillations equals an integral multiple of the rf frequency. n is the step index.

characteristics at threshold V_T as the n = 0 step, and the next step at higher dc fields as the n = 1 step, etc. The n = 1 step height δV, as defined in Fig. 11, in general first increases with increasing V_{ac} and then decreases. The position of the n = 1 step corresponds to a dc current <I> which yields an intrinsic oscillation of frequency $f_1 = \omega/2\pi$. As is apparent from Fig. 11, the <I> value where the n = 1 step occurs decreases with increasing V_{ac}. This is a consequence of excess dc current induced by the application of the rf field.[34] Harmonic steps corresponding to n = 2 (where $f_1 = 2\omega/2\pi$) are also apparent in Fig. 11. In a number of cases, subharmonic steps, corresponding to n = 1/2 (i.e. where $f_1 = \omega/4\pi$), are also observed. The steps are an interference effect between the intrinsic current oscillations and the externally applied rf excitation. Recent experiments[35] have shown that the magnitudes of the steps are directly proportional to the observed amplitude of the current oscillations, which is highly sample dependent.

Experiments analogous to those shown in Fig. 11 may be performed at different rf frequencies. A fairly complete set of results for $\delta V(n = 1)$ is shown in Fig. 12 for $NbSe_3$. It is

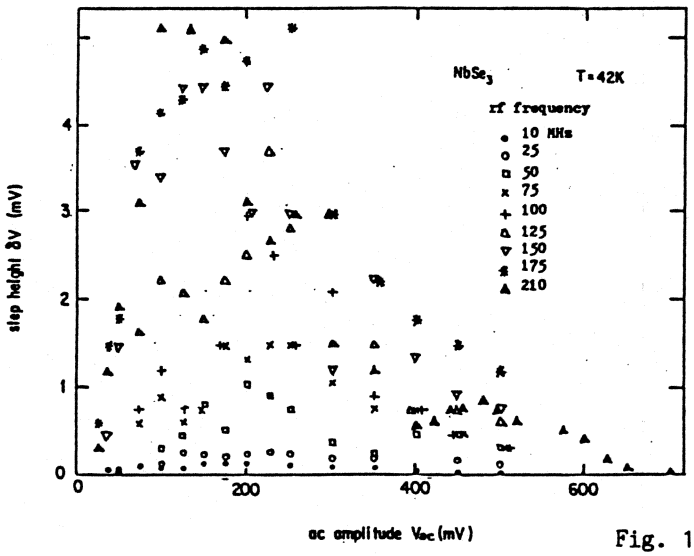

Fig. 12
Height of the n = 1 Shapiro step as a function of rf amplitude in $NbSe_3$.

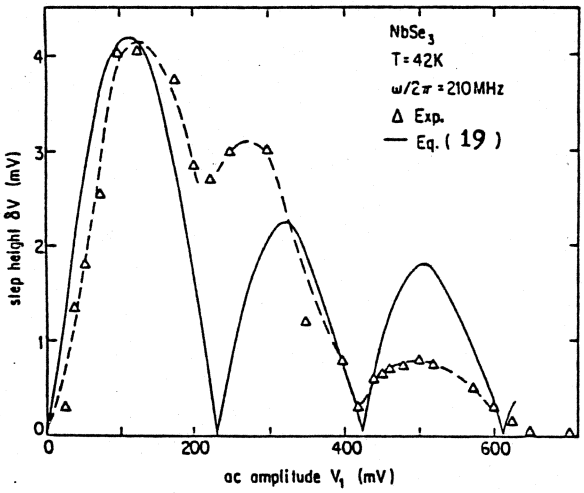

Fig. 13
Height of the n = 1 Shapiro step as a function of rf amplitude in $NbSe_3$. The rf frequency is 210 MHz. The dashed line is a guide to the eye; the solid line is Eq.(19).

apparent that in general larger effects are observed for higher frequencies ω. In Fig. 13 we isolate the 210 MHz data of Fig. 12 for clarity. We see that δV resembles a decaying oscillatory function, with well-defined maxima and minima.

The maximum value achieved, δV_{max}, on the first "peak" in Fig. 13 is approximately 4 mV. This value depends on ω, as demonstrated in Fig. 14. The data of Fig. 14 suggests a possible saturation of δV_{max} near 200 MHz, although data at higher frequency is needed to confirm this conjecture.

We may analyze the step phenomena in terms of Eq.(2). The analysis will rest heavily on the close correspondence between Eq.(2) and the equation describing a shunted Josephson junction. The substitution $\vartheta = Qx$ allows Eq.(2) to be reduced to the dimensionless form

$$\frac{d^2\theta}{dt^2} + \bar{\Gamma}\frac{d\theta}{dt} + \sin\theta = \frac{E}{E_T} \tag{16}$$

where $\bar{\Gamma} = 1/\omega_0\tau$, $E_T = (\lambda/2\pi)(m\omega_0^2/e)$ and time is measured in units of ω_0^{-1}. Eq.(16) is formally identical to the Stewart-McCumber equation for a resistively shunted Josephson junction[36],

$$\frac{d^2\phi}{dt^2} + G\frac{d\phi}{dt} + \sin\phi = \frac{I}{I_J} \tag{17}$$

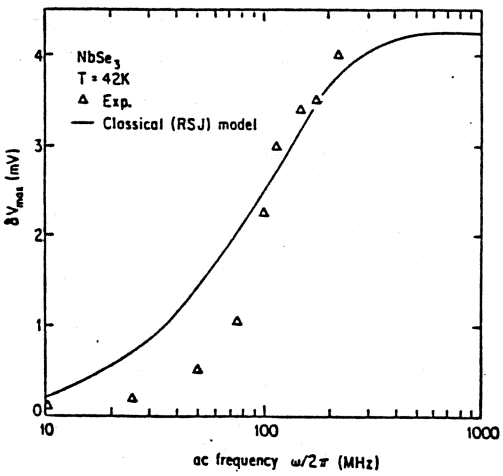

Fig. 14
Maximum height achieved for the n = 1 Shapiro step in $NbSe_3$, as a function of rf frequency. The maximum refers to the first peak (see text). The solid line is the prediction of Eq.(2) in the overdamped limit.

where ϕ is the phase difference across the junction, I is the current through the junction, and $G = (RC\omega_J)^{-1}$ where R and C are the resistance and capacitance of the junction, and $\omega_J = 2eI_J/C\hbar$. I_J is the dc Josephson critical current, and time is measured in units of ω_J^{-1}. The correspondence between classical CDW motion and Josephson properties has been discussed by various authors.[37] With the above analogy, the current oscillations and narrow-band noise for CDW transport corresponds to the ac Josephson effect.

One of the early evidences for Josephson effects was the observation[38] of so-called Shapiro steps-- a driving current of the form $I = I_{dc} + I_{ac}\cos(\omega t)$ will produce steps in the dc I-V characteristics of the junction whenever the junction voltage $\langle V \rangle$ equals $n\hbar\omega/2e$, where n is an integer. Steps corresponding to half integral values of n are also possible under certain conditions. The steps are a direct consequence of the ac Josephson effect. By explicitly solving Eq.(17) in the high frequency ($\omega >> 2eI_JR/\hbar$) limit, computer simulations and analytic approximations show[39,40] that the height of the n^{th} step is given by

$$\delta I \simeq I_J(\omega=0)\ 2\left|J_n[I_{ac}/\omega G\ I_J(\omega=0)]\right| \qquad (18)$$

where J_n is the Bessel function of order n. In the low frequency limit, where the capacitance of the junction is neglected, computer calculations[39,40] have yielded solutions for δI which closely resemble Bessel functions.

The mathematical equivalence of Eqs.(16) and (17) allows us to adapt the result of Eq.(18) to CDW transport. The height of the Shapiro-like steps in Fig. 11 is then given by

$$\delta V \simeq \beta_V\ V_T(\omega=0)2\left|J_n[V_{ac}\omega_0^2\tau/\omega V_T(\omega=0)]\right| \qquad (19)$$

in the high frequency limit. The parameter β_V represents the volume fraction of the $NbSe_3$ sample which responds collectively to

the external field. The solid line in Fig. 11 is Eq.(19) with chosen parameters $\omega_0^2\tau$ = 503 MHz and β_V = 0.17. The positions of the maxima and minima of the Bessel function of Eq.(19) are in remarkable agreement with the experimental data, and the crossover frequency is consistent with that obtained from the frequency dependence of the low-field ac conductivity. The value β_V = 0.17 indicates that a large fraction of the sample is responding coherently to the external perturbation. Analysis of similar data for other NbSe- samples has yielded values of β_V as high as 0.60, which corresponds to 60% of the sample being phase coherent. Typical values of β_V for TaS are 0.05, indicating a 5% volume phase coherence. At low frequencies Eq.(19) is inappropriate for an overdamped system. Neglecting the first term in Eq.(17) yields the standard RSJ model with negligible capacitance. In the CDW case this corresponds to zero inertia. In this limit, the value of δV_{max} is strongly frequency dependent. The solid line in Fig. 14 is the frequency dependence of δV_{max} as calculated for the RSJ model[36,40] in the overdamped limit, and adapted to Eq.(16). There are no adjustable parameters in this fit.

Although the above discussion has used Eq.(2) as a basis, a similar analysis should be possible within the framework of the tunneling model proposed by Bardeen.[12] The oscillation frequency there appears in the wave function of the moving CDW in a natural way. For a coupled electron-phonon system, moving with drift velocity v_d, the energy difference corresponding to $+k_F$ and $-k_F$ is given by

$$\delta\varepsilon \simeq \frac{\partial\varepsilon}{\partial v}v_d = \frac{\partial\varepsilon}{\partial k}\frac{\partial k}{\partial v}v_d \simeq 2v_F\, m^* v_d \qquad (20)$$

With $v_F = \frac{\hbar\pi}{m^*\lambda}$ one obtains $\delta\varepsilon = 2k_F\hbar v_d$. Hence the fundamental oscillation frequency corresponds to $f_1 2\pi\hbar = 2k_F\hbar v_d$, with an oscillation amplitude given by Eq.(9). These oscillations will interfere with incoming photons of frequency ω and energy $\hbar\omega$.

3.2 Ac Conductivity in the Presence of a dc Bias

Interference effects are also apparent in the low-field ac conductivity $\sigma(\omega)$, when a bias field exceeding E_T is applied. Again the dc-induced coherent current oscillations play a fundamental role. Fig. 15 shows both the real part of $\sigma(\omega)$ and

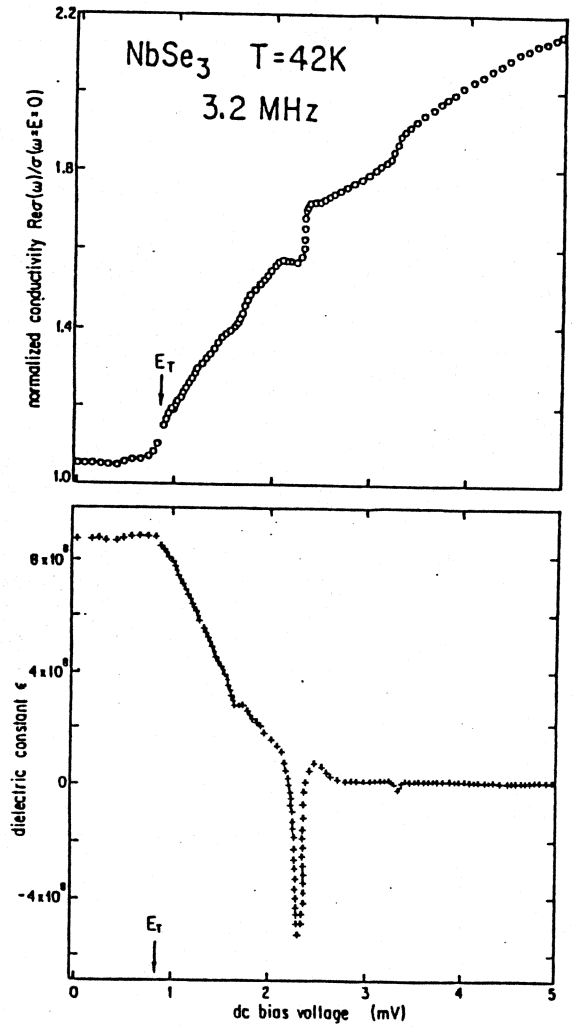

Fig. 15a
Real part of low-field ac conductivity in $NbSe_3$, as a function of dc bias voltage. The ac conductivity is measured at 3.2 MHz. E_T is the threshold field for the onset of non-linear dc conduction.

Fig. 15b
Ac dielectric constant of $NbSe_3$ as a function of dc bias voltage. The dielectric constant is measured at 3.2 MHz. E_T is the threshold field for the onset of non-linear dc conduction.

the ac dielectric constant $\varepsilon(\omega)$ as functions of dc bias, measured on $NbSe_3$. The dc bias has little effect below threshold, while strong anomalies are observed in both $Re\sigma(\omega)$ and $\varepsilon(\omega)$ in the non-linear conductivity region. These anomalies correspond to bias fields where the ac frequency $\omega/2\pi$ equals the frequency of the dc-induced current oscillations f_1, or a subharmonic or harmonic of f_1. If ω is increased, the anomalies occur at higher bias fields, as expected from Eq.(5). This is illustrated in Fig. 16, where $\varepsilon(\omega)$ is plotted for various values of ω as a function of dc bias. Similar anomalies are observed if E_{dc} is fixed above E_T, and $\sigma(\omega)$ is measured as a function of ω.

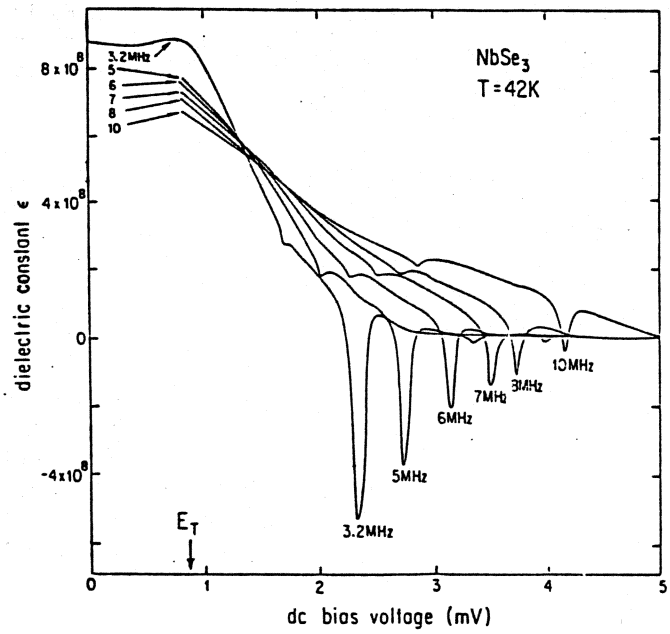

Fig. 16
Ac dielectric constant of $NbSe_3$ as a function of dc bias voltage. The dielectric constant is measured at various ac frequencies between 3 and 10 MHz. E_T is the threshold voltage for the onset of non-linear dc conduction.

If the generation of dc-induced current oscillations is assumed independent of the applied (low amplitude) rf field, the interference effects in Figs. 15 and 16 may be easily analyzed by applying classical rf circuit theory. Clearly the assumption of independence is inappropriate in a quantum description of the dynamics. In terms of a classical approach, the sample response to a purely ac low amplitude driving field $V_{ac}\sin\omega t$ can be approximated by $R\sin(\omega t+\theta)$, where R is a constant and θ reflects the out-of-phase component of the response. A purely dc driving field with $V_{dc} > V_T$ will produce a current response $C + Ng(2\pi f_1 t+\phi)$ where C is the time-averaged response and g is a periodic function of time with period $(2\pi f_1)^{-1}$ and of unit amplitude. Assuming independent behavior, the current response to a combined driving field of the form given by Eq.(15) will be

$$I = R\sin(\omega t+\theta) + N\,g(2\pi f_1 t+\phi) \tag{21}$$

where the time averaged component of the response has been subtracted. Approximating the coherent current oscillation by a sinusoidal function, and assuming $\omega/2\pi = f_1$ for strongest interference, we obtain a response

$$I = R\sin(\omega t+\theta) + N\sin(\omega t+\phi)\ . \tag{22}$$

From Fig. 16, the strong inductive dip in $\varepsilon(\omega)$ corresponds to a bias voltage V_{dc} where, in the absence of interference effects, $\varepsilon(\omega)$ is approximately zero. Thus, to analyze this dip we may set $\theta = 0$ in Eq.(22). The total phase difference β between the ac driving field and the response is then

$$\beta = \tan^{-1}\left[-\frac{N\sin\phi}{R+N\cos\phi}\right]\ . \tag{23}$$

Setting the phase-locking angle ϕ equal to the empirically determined value $\pi/2$ (which may also be determined from energy considerations), and using for R and N the measured response amplitudes, we obtain $\beta = 0.14$. This corresponds to a 4 MHz value of $\epsilon(\omega) = -7.66 \times 10^8$, in good agreement with the measured 4 MHz value -5.5×10^8 at the center of the inductive peak in Fig. 15. A similar analysis of Re $\sigma(\omega)$ predicts a step height $\Delta\sigma/\sigma_0 = 1.5$ for the dominant 4 MHz step, which again agrees favorably with the measured value 1.3.

The finite widths of the steps in Re $\sigma(\omega)$ and of the inductive dips in $\epsilon(\omega)$ indicate that interference effects occur over a small but finite range of noise frequencies for fixed ω. In a discussion of related synchronization effects in the differential resistivity of $NbSe_3$, Richard et al[16] have calculated the frequency width for which frequency locking will occur in a single domain. They obtain for the extreme E_{dc} value

$$E_{dc} - E_A + E_T\left[\frac{E_{ac}}{2E_A}\right] \tag{24}$$

where E_A is that bias field which yields a fundamental noise frequency $f_1 = \omega/2\pi$. Eq.(24) predicts a width of the strong indictive dip in $NbSe_3$ at 4 MHz of $2(E_{dc}-E_A) = V_T(V_{ac}/V_A) = .27$ mV, in excellent agreement with the observed width 0.26 mV in Fig. 15.

The strong interference effects observed in $NbSe_3$ are thus adaquately explained in terms of classical electromagnetic interference phenomona.

A recent model of CDW transport by Sneddon, Cross, and Fisher[10] treats the problem using a classical, hydrodynamic analysis. The CDW is assumed deformable and internal degrees of freedom are taken into account. The equation of motion is

$$m\ddot{u}(\vec{r},t) + \int D(\vec{r}-\vec{r}')u(\vec{r},t)d^3r' + \lambda\dot{u} - en_cE = - en_c(r)\frac{\partial}{\partial z}\Phi\left(\vec{r}+u(\vec{r},t)\right) \tag{25}$$

where u is the local CDW distortion, $n_c e$ is the electron charge density, and Φ is the CDW potential. The model predicts that, in the infinite-volume limit, coherent current oscillations are absent, but interference effects exist. The interference effects shown in Figs. 15 and 16 for $NbSe_3$ reflect a direct interaction between the current oscillations (which themselves may be a finite-size effect) and the external field. Hence the applicability of the hydrodynamic solution to this data is questionable.

In TaS_3, where the current oscillations are typically an order of magnitude smaller in amplitude than in $NbSe_3$, interference effects are not as apparent, as can be seen from Fig. 17. This figure shows $\sigma(\omega)$ as a function of dc bias in TaS_3.

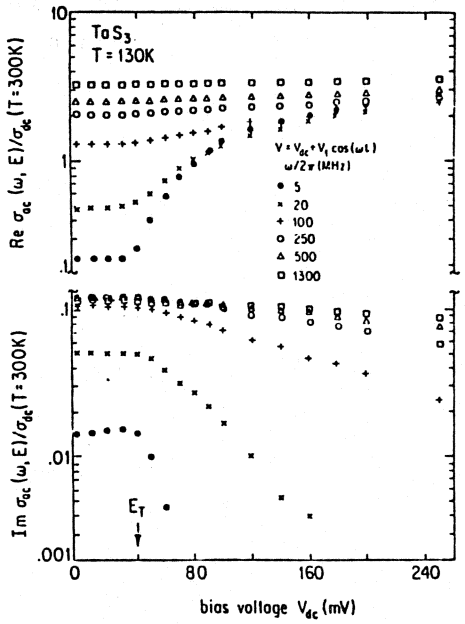

Fig. 17
Ac conductivity of TaS_3 as a function of dc bias voltage, measured at various ac frequencies. Both the real and immaginary parts ofthe conductivity are shown. E_T represents the threshold field for the onset on non-linear dc conduction.

4. SWITCHING

Switching refers to a sharp jump in the dc I-V characteristics at threshold. It is observed in $NbSe_3$ at low temperatures, and in other CDW systems as well (to date excluding

TaS_3). Fig. 18 shows the phenomenon in $NbSe_3$. At high temperatures (T = 42 K) the I-V curves are smooth at E_T with no outstanding features. At slightly lower temperatures a knee is observed in the I-V curves near E_T. The knee becomes sharper with lowering temperature, and near approximately 36 K a jump or switch is observed from the ohmic to the non-linear conductivity regime. As the temperature is further lowered, the switch becomes more well-defined, and near 28 K it shows clear hysteresis behavior for increasing and decreasing currents through the threshold value. The hysteresis loop becomes larger with decreasing temperature, and it can eventually encompass the region $I_{dc} = 0$. At low temperatures the switch is sharp and the hysteresis loop is well defined. At intermediate temperatures, however, the switch is not as sharp, and the system briefly oscillates or "fibrillates" between the conducting and non-conducting states. This is shown more clearly in Fig. 19, where portions of the I-V curves near threshold are shown at two temperatures.

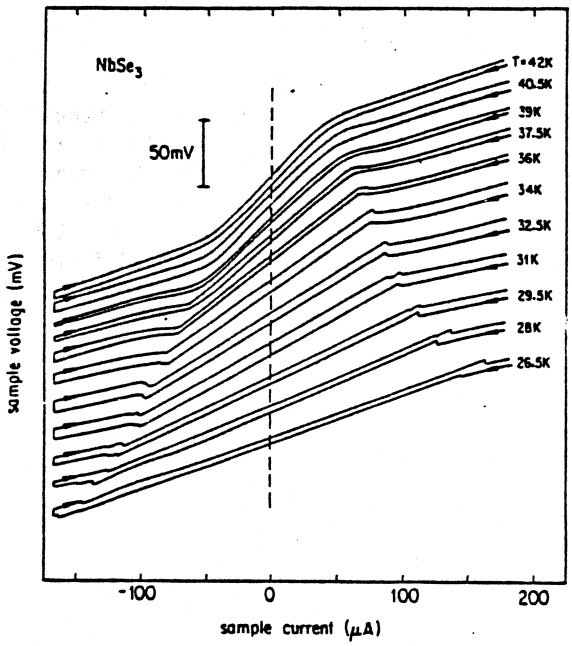

Fig. 18
Dc I-V traces for $NbSe_3$ at selected temperatures. For each temperature, both a forward and reverse current sweep is shown.

Pulsed experiments[41] have shown that the switching at E_T is not instantaneous, and two characterestic times are involved in

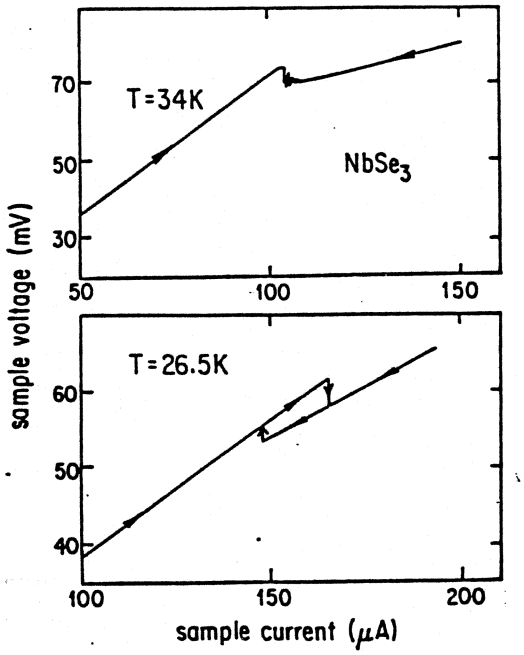

Fig. 19
Detail of dc I-V characterestics on $NbSe_3$ near threshold. the arrows indicate the direction of current sweep. At low temperatures, the switching is hysteretic.

the switching process. First, as the threshold current I_T is achieved at time t = 0, there is a finite time, T_s, before the switching actually commences. Second, the switch itself is of duration t_s. t_s is typically a few microseconds, while Ts may be up to several hundred microseconds, depending on the ratio I/I_T at time t = 0. I is the appplied (pulsed) current. The switching is not a deterministic process, i.e. for fixed I, T_s is not uniquely defined. Rather, the switching probability $P(T_s)$ is well described by

$$P(T_s) = \frac{c}{\pi} \frac{1}{1+c^2(T_s-\bar{T}_s)^2} \qquad (26)$$

where c is a constant and $\bar{T}_s$ is the mean time before switching.

Neither the single-particle or hydrodynamic classical model, nor the tunneling model, describes switching at threshold in a self-consistent fashion. Switching and hystersis are easily incorporated into classical descriptions by assuming a non-negligible inertial term. This assumption is however not

consistent with the low-field ac response, which indicates an overdamped system. It is, on the other hand, important to realize that the classical and quantum models discussed above are zero temperature formulations, and that they neglect any possible distributions of CDW segments as might arise from inhomogenities or grain boundaries, etc. The switching and hysteresis may be related to a distribution of CDW domains in that various CDW regions have first to be coupled together before a current-carrying CDW state can develop. The switching phenomenon observed is then associated with the finite time required for coupling after the application of a driving field. The situation is similar to that observed in coupled Josephson junctions, and in granular superconductors.[42]

A recent model of CDW conduction by Joos and Murray[43] assumes the specimen to be composed of a large and finite number of domains, where the domains are either conducting or non-conducting. Hence, the model is analogous to the kinetic Ising model. By assuming CDW conduction occurs only through a continuous channel of conducting domains, Joos and Murray find switching effects with a probability distribution in excellent agreement with Eq.(26) and with experiment.[41] As discussed earlier, domain coupling also appears to be an important consideration in analyzing the time dependence of coherent current oscillations.

An interesting observation[44] regarding switching is that, following a well-defined switch, the <u>differential</u> resistance dV/dI becomes <u>independent</u> of E. This is illustrated in Fig. 20 for $NbSe_3$. The differential resistance thus obtained just after the switch corresponds to the high-field limit of the differential resistance, which is equivalent to the high field limit of the pure resistance. The "high-field" CDW state is thus achieved immediately following the switch. This is illustrated in Fig. 21 for $NbSe_3$ at low temperatures.

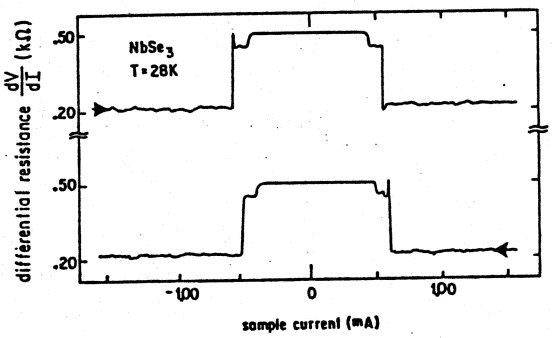

Fig. 20
Differential resistance dV/dI of $NbSe_3$ at low temperature. Data for both forward and reverse current sweeps is shown. The differential resistance is independent of electric field before and after the switch.

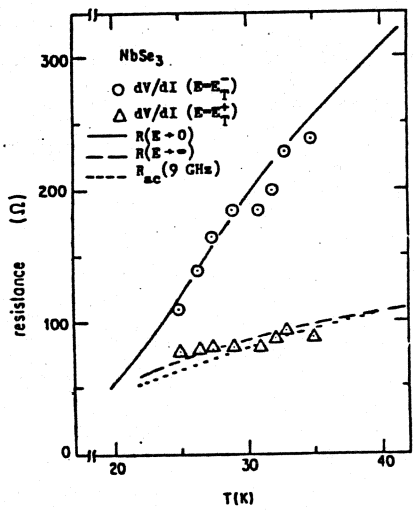

Fig. 21
Differential resistance dV/dI for $NbSe_3$ before and after switching, measured at selected temperatures. Also shown are the high field limit of the resistance, and the ac resistance measured at microwave frequencies. The microwave data is from ref. 2.

5. CONCLUSION

We have here discussed coherent oscillations, interference effects, and switching associated with the CDW condensate. The coherent current oscillations in $NbSe_3$ and TaS_3 yield strong

evidence that the sample volume is to a large extent phase coherent for typical crystal dimensions (1μm x 10μm x 1 mm). This is supported by the analysis of interference effects when both dc and ac driving fields are applied. However, the time dependence of the current oscillations, along with the switching phenomenon, indicates an important role played by domain structure. How domain coupling is accomplished, whether by long-range order or simply by the driving current passing through the specimen, is unclear.

The coherent oscillation phenomenon appears consistent with a sliding motion of the CDW over the hills and valleys of the pinning potential, but inconsistent with soliton transport or oscillations from macroscopic quantum states analogous to Josephson oscillations. The observed interference effects are a direct result of coupling between external ac perturbations and internally generated current oscillations. Hence the interference effects do not correspond to those predicted by a hydrodynamic pertubation theory approach. However, recent experiments[35] indicate that these internal modes (applicable to an infinite volume sample and hence excluding finite-size effects) can be excited in appropriate limits, irrespective of the current oscillations.

An interesting point with regard to Shapiro steps in CDW systems is the finite width of the steps. In Josephson junctions, for example, analogous steps are extremely sharp (although they can be smeared somewhat by temperature effects). In CDW systems, the finite step width is directly related to the rounding of the I-V characteristics near threshold. For example, recent studies[44] have shown that if the threshold is very sharp, then the Shapiro steps are equally sharp. This is dramatically realized in $NbSe_3$ at low temperatures where switching occurs not only at threshold, but at each successive Shapiro step if an rf field is present.[44] Whether the rounding near threshold at high temperatures in $NbSe_3$ and in TaS_3 is due to an effective noise term or is intrinsic to CDW depinning, remains to be seen.

6. ACKNOWLEDGEMENTS

The experiments described in this presentation were performed together with G. Gruner, W. G. Clark, and R. Hall. I wish to thank J. Bardeen, A. Zawadowski, A. Portis, and L. Sneddon for beneficial discussions and interactions. This research was supported in part by NSF Grant DMR 81-03085 (UCLA) and a Grant from the UC Berkeley Campus Committee on Research.

7. REFERENCES

1. P. Monceau, N. P. Ong, A. M. Portis, A. Meerschaut, and J. Rouxel, Phys. Rev. Lett. 37, 602 (1976)

2. N. P. Ong and P. Monceau, Phys. Rev. B16, 3443 (1977)

3. G. Gruner, L. C. Tippie, J. Sanny, W. G. Clark, and N. P. Ong, Phys. Rev. Lett. 45, 935 (1980)

4. C. M. Jackson, A. Zettl, G. Gruner, and A. H. Thompson, Solid State Commun. 39, 531 (1981)

5. A. Zettl and G. Gruner, Phys. Rev. B25, 2081 (1982)

6. R. M. Fleming and C. C. Grimes, Phys. Rev. Lett. 42, 1423 (1979)

7. G. Gruner, A. Zettl, W. G. Clark, and A. H. Thompson, Phys. Rev. B23, 6813 (1981)

8. For a review see G. Gruner and A. Zettl, "Charge Density Wav Conduction: A Novel Collective Transport Phenomenon in Solids", Adv. Phys. (in press)

9. H. Frohlich, Proc. Roy. Soc. London, A223, 296 (1954)

10. L. Sneddon, M. C. Cross, and D. S. Fisher, Phys. Rev. Lett. 49, 292 (1982)

11. G. Gruner, A. Zawadowski, and P. M. Chaikin, Phys. Rev. Lett. 46, 511 (1981)

12. J. Bardeen, Phys. Rev. Lett. 45, 1978 (1980)

13. M. Weger, G. Gruner, and W. G. Clark, Solid State Commun. 44, 1179 (1982)

14. A. Zettl and G. Gruner, Phys. Rev. B (in press)

15. See G. Gruner "Frequency and Electric Field Dependent Transport due to Charge Density Wave Condensates", (this volume)

16. P. Monceau, J. Richard, and M. Renard, Phys. Rev. B25, 931 (1982); J. Richard, P. Monceau, and M. Renard, Phys. Rev. B25, 948 (1982)

17. P. Monceau, J. Richard, and M. Renard, Phys. Rev. Lett. 45, 43 (1980)

18. J. Bardeen, E. Ben-Jacob, A. Zettl, and G. Gruner, Phys. Rev. Lett. 49, 493 (1982)

19. N. P. Ong, Phys. Rev. B18, 5272 (1978); G. X. Tessema and N. P. Ong, Phys. Rev. B23, 5607 (1981)

20. C. Roucau, R. Ayroles, P. Monceau, L. Guemas, A. Meerschaut, and J. Rouxel, Phys. Stat. Sol. A62, 483 (1980)

21. K. Tsutsumi, T. Sambongi, S. Kagoshima, and I. Ishiguro, J. Phys. Soc. Japan, 44, 1735 (1978)